Monthly Notices
of the
ROYAL ASTRONOMICAL SOCIETY

MNRASL **439,** L51–L55 (2014)
Advance Access publication 2014 January 16

doi:10.1093/mnrasl/slt178

ULASJ1234+0907: the reddest type 1 quasar at $z = 2.5$ revealed in the X-ray and far-infrared*

Manda Banerji,[1]† A. C. Fabian[2] and R. G. McMahon[2,3]

[1]*Department of Physics & Astronomy, University College London, Gower Street, London WC1E 6BT, UK*
[2]*Institute of Astronomy, University of Cambridge, Madingley Road, Cambridge CB3 0HA, UK*
[3]*Kavli Institute for Cosmology, University of Cambridge, Madingley Road, Cambridge CB3 0HA, UK*

Accepted 2013 December 6. Received 2013 November 29; in original form 2013 November 14

ABSTRACT

We present *Herschel* and *XMM–Newton* observations of ULASJ1234+0907 ($z = 2.503$), the reddest broad-line type 1 quasar currently known with $(i - K)_{AB} > 7.1$. *Herschel* observations indicate that the quasar host is a hyperluminous infrared galaxy with a total infrared luminosity of $\log_{10}(L_{\rm IR}/{\rm L}_{\odot}) = 13.90 \pm 0.02$. A greybody fit gives a dust temperature of $T_{\rm d} = 60 \pm 3$ K assuming an emissivity index of $\beta = 1.5$, considerably higher than in sub-millimeter bright galaxies observed at similar redshifts. The star formation rate is estimated to be $>2000\,{\rm M}_{\odot}\,{\rm yr}^{-1}$ even accounting for a significant contribution from an active galactic nucleus (AGN) component to the total infrared luminosity or requiring that only the far-infrared luminosity is powered by a starburst. *XMM–Newton* observations constrain the hard X-ray luminosity to be $L_{2-10\,{\rm keV}} = 1.3 \times 10^{45}\,{\rm erg\,s}^{-1}$, putting ULASJ1234+0907 among the brightest X-ray quasars known. Through very deep optical and near-infrared imaging of the field at subarcsecond seeing, we demonstrate that despite its extreme luminosity, it is highly unlikely that ULASJ1234+0907 is being lensed. We measure a neutral hydrogen column density of $N_{\rm H} = 9.0 \times 10^{21}\,{\rm cm}^{-2}$ corresponding to $A_{\rm V} \sim 6$. The observed properties of ULASJ1234+0907 – high luminosity and Eddington ratio, broad lines, moderate column densities and significant infrared emission from reprocessed dust – are similar to those predicted by galaxy formation simulations for the AGN *blowout* phase. The high Eddington ratio, combined with the presence of significant amounts of dust, is expected to drive strong outflows due to the effects of radiation pressure on dust.

Key words: galaxies: active – quasars: general – quasars: individual.

1 INTRODUCTION

Since the discovery of the correlation between the mass of the galactic bulge in galaxies and the mass of their central black holes (Magorrian et al. 1998), understanding the link between the formation and evolution of massive galaxies and their supermassive black holes (SMBH; 10^5–$10^{10}\,{\rm M}_{\odot}$) has become one of the most important problems in both galaxy formation and extreme astrophysics. The realization that an active SMBH or active galactic nucleus (AGN) plays a fundamental role in determining the final stellar mass of the galactic bulge has wide implications and has led to the ubiquitous adoption of AGN *feedback* in many galaxy formation models (Croton et al. 2006). In cosmological simulations, the most massive galaxies in the Universe are assembled at high redshift through gas-rich mergers of smaller systems (Hopkins et al. 2008). The merger is expected to induce a far-infrared (FIR)-luminous starburst, which enshrouds the galaxy in dust therefore obscuring it completely at ultraviolet (UV) and optical wavelengths. The high gas densities in the merging starburst feed accretion on to the central black hole, which is initially also dust obscured. As radiative pressure on the dust grains begins to clear the dust and gas away during the *blowout* phase (Di Matteo, Springel & Hernquist 2005), the central AGN is revealed as a UV-luminous quasar. Several indirect lines of evidence suggest that powerful starbursts and luminous quasars occur in the same galaxies (Coppin et al. 2008; Hickox et al. 2012) and there is observational evidence at low redshifts for dusty quasars residing in mergers (Urrutia, Lacy & Becker 2008). However, direct observational evidence for starburst galaxies at high redshifts transitioning to UV-luminous quasars has remained elusive.

In Banerji et al. (2012, 2013) – B12, B13 hereafter – we used infrared surveys to identify 14 extremely massive, luminous, dusty broad-line quasars at $z \sim 2$ that could represent galaxies caught during the AGN blowout phase. This new population of quasars is too dusty to be present in optical surveys like the Sloan Digital

** Herschel* is an ESA space observatory with science instruments provided by European-led Principal Investigator consortia and with important participation from NASA.

† E-mail: m.banerji@ucl.ac.uk

Sky Survey (SDSS) that have so far been used to identify the most luminous quasars in the Universe. The reddest and most intrinsically luminous quasar in our current sample is ULASJ1234+0907 at $z = 2.503$. Our spectroscopic observations in B12 detected very broad Hα emission from this quasar signifying the presence of an extremely massive SMBH ($\sim 3 \times 10^{10}\,M_{\odot}$) and/or significant outflows that could be broadening the Hα line. This broad emission line also supports the interpretation that the dust responsible for the red colours of the quasar originates on large scales within the quasar host, rather than in a molecular torus. The dust extinction implied by our spectral energy distribution (SED) fit to the broad-band colours of ULASJ1234+0907 is $A_V = 6$ mag even accounting for the effect of the large Hα equivalent width on the $(H - K)$ colour (see B12 for details).

If ULASJ1234+0907 is being observed in the AGN blowout phase, the next step is to look for evidence for a massive starburst quasar host. In this Letter, we present detailed multiwavelength observations of this quasar. X-ray observations with *XMM–Newton* allow us to directly detect the primary accreting power source, while FIR and submillimeter observations with *Herschel* and Submillimetre Common-User Bolometer Array (SCUBA-2) are used to place the first constraints on the quasar host galaxy. Throughout this Letter, we assume a flat Λ cold dark matter cosmology. All magnitudes are on the AB system with conversion from the Vega system using zero-point offsets for UKIDSS and *WISE* photometry from Hewett et al. (2006) and Cutri et al. (2012)

2 OBSERVATIONS

2.1 Optical and near-infrared imaging

We conducted *i*-band imaging of the quasar using the Wide-Field Camera on the 2.5 m ISAAC Newton Telescope (INT) in 2008 April and May. The total exposure time was 85 min. The six individual exposures were reduced, stacked and photometrically calibrated on to the SDSS *AB* system following González-Solares et al. (2011). ULASJ1234+0907 was undetected in the stacked *i*-band image (Fig. 1) with a 5σ magnitude limit of 25.15 giving an $(i - K)$ colour of >7.1. ULASJ1234+0907 is therefore among the reddest extragalactic sources known. Fig. 2 of B12 shows the $(i - K)$ colours of various well-known extremely red objects. The reddest quasar from that figure: PKSJ0132 which was the reddest quasar previously known (Gregg et al. 2002) has an $(i - K) = 4.2$, almost 3 mag bluer than ULASJ1234+0907.

We conducted K_S-band observations of ULASJ1234+0907 using the ISAAC camera on the Very Large Telescope. Data were taken in 2013 March under photometric conditions and in very good seeing of <0.5 arcsec The observations were taken using 15 dithered exposures of 60 s and reduced using standard European Southern Observatory (ESO) tools provided as part of the GASGANO package. The resulting *K*-band image shown in Fig. 1 goes down to a 10σ depth of 23.2.

2.2 FIR and submillimeter photometry: *Herschel* and SCUBA-2

Herschel (Pilbratt et al. 2010) Director's Discretionary Time observations were obtained in 2012 December with PACS (Poglitsch et al. 2010). Data were taken in mini scanmap mode using a scan speed of 20 arcsec s^{-1} and a scan leg length of 3 arcmin with exposure times in the range of 444–895 s at 70, 100 and 160 μm. PACS maps were produced with the default pixel scale of 1.4, 1.7 and 2.8 arcsec at 70, 100 and 160 μm, respectively, using *Herschel*

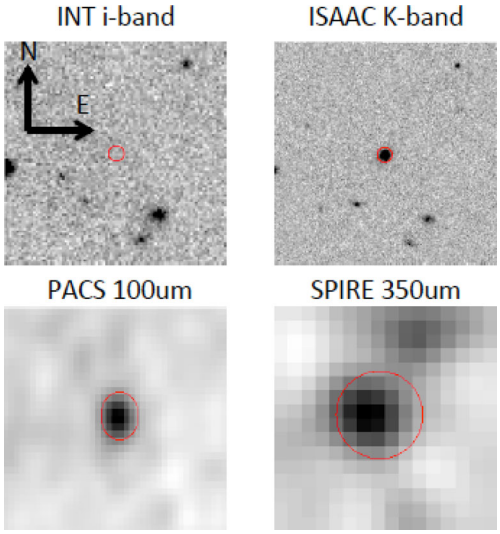

Figure 1. Multiwavelength images of ULASJ1234+0907 taken with various instruments. The INT *i*-band and ISAAC K_S-band images are 30 × 30 arcsec, while the *Herschel* cut-outs are 2 × 2 arcmin in size. In all cases, the directions of north and east are as specified in the *i*-band image. The quasar position is circled in all images with the size of the circle roughly corresponding to the beam size at that particular wavelength.

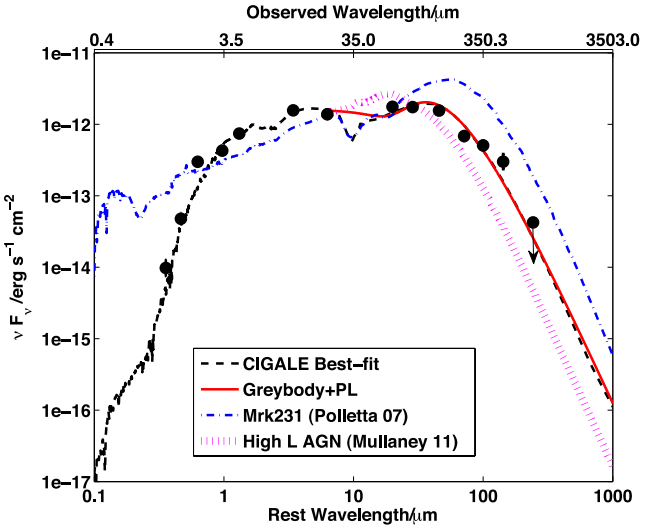

Figure 2. Best-fitting SED to the observed photometry of ULASJ1234+0907 at $z = 2.503$ in units of νF_ν. The dashed line is for the best-fitting CIGALE SED which includes both AGN and starburst components, while the solid line denotes the simple greybody plus MIR power-law fit to the data. We also show the SEDs of Mrk231 from Polletta et al. (2007) (dot–dashed line) and the high-luminosity AGN from Mullaney et al. (2011) (dotted line). All SEDs have been scaled to match the rest-frame flux density of ULASJ1234+0907 at ∼6 μm which corresponds to the observed-frame *WISE* 22 μm band.

Level 1 data products and the map-making software SCANAMORPHOS (Roussel 2012). Fluxes were measured by performing annular aperture photometry at the quasar position using apertures of 5.5, 5.6 and 10.5 arcsec at 70, 100 and 160 μm, respectively. The background was measured using apertures of [20,25] arcsec at 70 and 100 μm, and [24,28] arcsec at 160 μm. Appropriate aperture corrections were applied to these fluxes (Poglitsch et al. 2010). Statistical errors on the fluxes were determined by taking the standard

Table 1. Summary of multiwavelength observations of ULASJ1234+0907 at $z = 2.503$.

Instrument and band	Flux density
INT *i*	<0.316 μJy (5σ)
WFCAM *Y*	<0.435 μJy (5σ)
WFCAM *J*	4.06 ± 1.10 μJy
WFCAM *H*	25.9 ± 4.9 μJy
WFCAM *K*	219.4 ± 6.1 μJy
WISE 3.4 μm	0.48 ± 0.02 mJy
WISE 4.6 μm	1.14 ± 0.04 mJy
WISE 12 μm	6.27 ± 0.23 mJy
WISE 22 μm	10.1 ± 1.6 mJy
Herschel-PACS 70 μm	41 ± 4 mJy
Herschel-PACS 100 μm	58 ± 6 mJy
Herschel-PACS 160 μm	83 ± 8 mJy
Herschel-SPIRE 250 μm	57 ± 9 mJy
Herschel-SPIRE 350 μm	59 ± 9 mJy
Herschel-SPIRE 500 μm	50 ± 12 mJy
SCUBA-2 850 μm	<12 mJy (3σ)

deviation of aperture fluxes calculated in blank fields on the combined maps. Systematic flux calibration errors of 5 per cent were added in quadrature to these. The final fluxes and errors are presented in Table 1, and the PACS cut-out at 100 μm is shown in Fig. 1.

Herschel-SPIRE data at 250, 350 and 500 μm are available as part of the *Herschel* Virgo Cluster Survey (HeViCS; Davies et al. 2010) in the V3 field. We used the Level 1 processed data from the *Herschel* Science Archive. Timeline fitting was performed on each of the four orthogonal scans within HIPE. In several cases, the timeline fitting produced fluxes for one of the scans that was inconsistent with the remaining scans at the level of 20 per cent. We therefore rejected the most discrepant scan from the set of four observations and took the final SPIRE flux to be the median value of the remaining scans. Colour corrections of 0.912, 0.916 and 0.901 at 250, 350 and 500 μm were applied, appropriate for a typical dusty source with spectral index $\alpha = 3$. The final fluxes are presented in Table 1. Error estimates from the timeline fitting were very similar from scan to scan: ∼8, 8 and 10 mJy at 250, 350 and 500 μm, respectively. Our final errors also include the calibration uncertainty assumed to be 7 per cent (Bendo et al. 2013).

SCUBA-2 service time observations (s12au01; PI: Banerji) were taken in 2012 April. The source was observed in *Daisy* mode for 20 min and the data were reduced using the SubMillimeter User Reduction Facility iterative map maker software to construct an 850 μm flux density map of the quasar using the default configuration parameters for blank fields. The reduced image has a mean rms of 4 mJy. The quasar was undetected in this 850 μm image leading to a 3σ upper limit of $S_{850} < 12$ mJy for ULASJ1234+0907.

2.3 X-ray observations

X-ray data for ULASJ1234+0907 were obtained using the European Photon Imaging Camera on the *XMM–Newton* satellite (Jansen et al. 2001). The total exposure time was 42 ks for the pn detectors and 52 ks for the MOS detectors. Thin filters were used. The total pn source count was 470. A spectrum was extracted in a 21.6 arcsec aperture around the target. The background was measured from the same chip at a radius of 1.2 arcmin from the source. The X-ray spectrum from the pn detector can be seen in Fig. 3. The MOS detectors are less sensitive, but the spectrum obtained from these is consistent with Fig. 3.

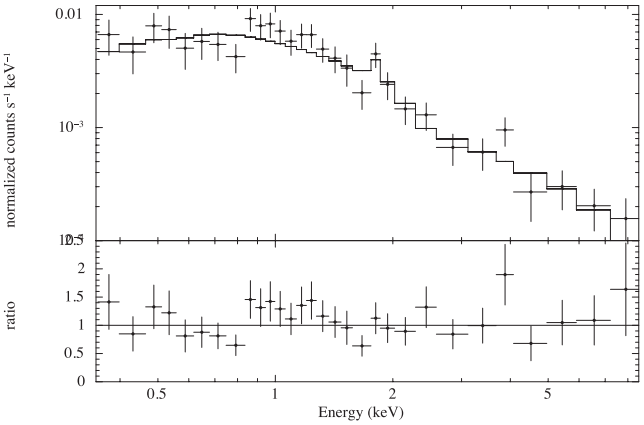

Figure 3. X-ray spectrum of ULASJ1234+0907 in the observed frame together with the best-fitting absorbed power-law model to this spectrum. The spectrum covers observed-frame energies of 0.4–8 keV corresponding to rest-frame energies of 1.4–28 keV.

3 ANALYSIS

3.1 SED fitting and star formation in ULASJ1234+0907

We fit an SED model to the observed photometry of ULASJ1234+0907 summarized in Table 1. Fitting the SED in the FIR requires us to disentangle the contribution of the AGN and the starburst to the total infrared luminosity. We adopt two approaches for the SED fitting. First, we use the publicly available SED fitting code CIGALE (Noll et al. 2009), which allows us to fit for both the AGN and starburst components at infrared wavelengths. In this code, the fractional contribution of the AGN to the total infrared luminosity is left as a free parameter in the fitting. The code uses the semi-empirical models of Dale & Helou (2002) to model the dust emission at infrared wavelengths. AGN templates can additionally be incorporated, and we adopt 32 AGN templates from the library of Fritz, Franceschini & Hatziminaoglou (2006), encompassing a range of torus opening angles, density parameters, optical depths and outer and inner radii of the dust clouds. We note that the inclusion of other AGN templates available within CIGALE does not significantly change our results.

Our second approach is simpler with fewer free parameters and allows direct comparison with greybody fits to the SEDs of other high-redshift galaxy populations. We use the code developed by Casey (2012) to fit a single temperature greybody and a power law of the form $S_\lambda \propto \lambda^\alpha$, to model the mid-infrared (MIR) emission at rest-frame wavelengths $\gtrsim 3$ μm. The power law approximates the contribution from an AGN-heated warm dust component.

Using the CIGALE fit, we find that the total infrared luminosity is $\log_{10}(L_{\rm TIR}) = 13.90 \pm 0.02$ with the AGN contribution to this IR luminosity fit to be 62 ± 4 per cent. The starburst luminosity is therefore $\log_{10}(L_{\rm SB}) = 13.5 \pm 0.1$ which translates to a star formation rate of $\sim 4500 \pm 900\,{\rm M}_\odot\,{\rm yr}^{-1}$ using the Kennicutt & Evans (2012) relation: ${\rm SFR} = 3.89 \times 10^{-44} \times L_{\rm SB}$ (erg s^{-1}). Despite the AGN dominating the infrared dust emission, the SED fitting indicates that this AGN cannot account for all of the infrared emission, and the host galaxy of ULASJ1234+0907 must also be forming stars at a prodigious rate. With a starburst luminosity of $> 10^{13}\,{\rm L}_\odot$, it can be classified as a hyperluminous infrared galaxy or HyLIRG.

In the case of the single greybody fit, we fix the dust emissivity index to $\beta = 1.5$ (Priddey et al. 2003) due to a lack of photometric data over the Rayleigh–Jeans tail of the SED. The

free parameters are the power-law slope, α in the MIR as well as the dust temperature. Although the AGN is expected to dominate the total infrared luminosity, the FIR luminosity between 40 and 300 μm can safely be attributed to a starburst (Rowan-Robinson 2000). We integrate our best-fitting single greybody SED between 40 and 300 μm and use this as a conservative estimate of the total amount of star formation. The infrared luminosity between 40 and 300 μm, $L_{40-300\,\mu m} = 1.3 \times 10^{13}\,L_{\odot}$ corresponding to a star formation rate of $\sim 2000 \pm 500\,M_{\odot}\,yr^{-1}$. The MIR power-law slope is relatively shallow: $\alpha = 1.03 \pm 0.03$, which is consistent with the presence of a significant warm dust component from AGN-heated dust. The best-fitting cold dust temperature is also higher than seen in most submillimeter galaxies: $T_d = 60 \pm 3$ K. The corresponding dust mass is $\log_{10}(M_{dust}/M_{\odot}) = 8.94 \pm 0.08$.

In Fig. 2, we also show the SED of the archetypal starburst/AGN composite galaxy Mrk231 in the local Universe which has been scaled to have the same flux density as ULASJ1234+0907 at a rest-frame wavelength of 6 μm. Finally, we plot the composite FIR SED of the high-luminosity ($\log(L_{2-10\,keV}) > 42.9$) X-ray AGN from Mullaney et al. (2011) again scaled to ULASJ1234+0907 at a rest-frame wavelength of 6 μm. ULASJ1234+0907 has a higher MIR-to-FIR flux ratio than Mrk231. The pure AGN SED on the other hand drops rapidly at rest-frame wavelengths of $\gtrsim$40 μm, whereas the SED of ULASJ1234+0907 extends to longer wavelengths and only begins to drop off at ∼60 μm. This excess cool dust emission relative to pure AGN could again be indicative of a starburst component. Further evidence for star formation is provided by the fact that the observed 500 μm data point is not particularly well fitted by the models and lies above the model SEDs. At the redshift of this quasar, the [C II] cooling line is in the SPIRE 500 μm band and can increase the broad-band flux by 20–40 per cent (Smail et al. 2011).

Our observations cannot directly rule out the presence of AGN-heated cool dust distributed at larger radii from the central black hole than the hotter dust responsible for the MIR emission. However, many FIR-luminous quasars at high redshift have been demonstrated to contain significant reservoirs of molecular gas, which is unambiguous evidence for star formation (Wang et al. 2010). Furthermore, we demonstrate below using X-ray observations of the quasar that the AGN bolometric luminosity inferred independently from the X-ray is significantly lower than the total infrared luminosity measured for this object. This once again hints that some additional source of heating apart from the AGN, is responsible for the reprocessed FIR dust emission. Regardless of the origin of the cool dust emission in the FIR, we conclude that ULASJ1234+0907 is among the most FIR-luminous broad-line quasars known.

3.2 X-ray spectrum

In Fig. 3, we plot the X-ray spectrum of ULASJ1234+0907 obtained using *XMM–Newton* together with the best-fitting model spectrum fit using XSPEC. The model includes Galactic absorption plus intrinsic absorption (at $z = 2.5$) acting on a power-law continuum with a narrow emission line at 6.4 keV to account for fluorescent Fe Kα. The total flux in the hard X-ray band covering 2−10 keV (observed frame) is 2.6×10^{-14} erg s^{-1} cm^{-2} from the model fit. The (source rest-frame) hard X-ray luminosity is therefore $L_{2-10\,keV} = 1.3 \times 10^{45}$ erg s^{-1} in our adopted cosmology. The best-fitting photon index is $1.68\pm^{0.25}_{0.22}$ and the inferred hydrogen column density is $N_H = (9.0\pm^{1.0}_{0.8}) \times 10^{21}$ cm^{-2}. This column density agrees with the extinction of $A_V = 6$ mag calculated from the near-infrared (NIR) broad-band colours in B12 assuming that the dust properties are similar to our own Milky Way. The X-ray observations therefore indicate that ULASJ1234+0907 is also among the most X-ray-luminous quasars known with a hard X-ray luminosity that is almost two orders of magnitude greater than Mrk231 and similar to the most powerful quasars in the Universe.

In the most powerful quasars accreting at close to the Eddington limit, the bolometric correction from the hard X-ray band is expected to be ∼50–100 (Elvis et al. 1994). This implies that the AGN bolometric luminosity of ULASJ1234+0907 is $\sim 1.3 \times 10^{47}$ erg s^{-1}. Even assuming that all of this luminosity is seen as reprocessed dust emission in the FIR, the shortfall in the total infrared luminosity calculated from the *Herschel* data is still $\sim 1.7 \times 10^{47}$ erg s^{-1}. If this *missing* infrared luminosity is to come from star formation, we now obtain an even more extreme star formation rate in the quasar host galaxy of $\sim 6800\,M_{\odot}\,yr^{-1}$.

The census of known AGN shows a remarkable lack of luminous, high Eddington ratio quasars that also have high columns of dust (Raimundo et al. 2010). These conditions are expected to drive strong outflows due to the effects of radiation pressure on the dust (Fabian 2012). The lack of very luminous, dusty quasars is perhaps not surprising given that most rapidly accreting quasars with high Eddington ratios have predominantly been selected at UV–optical wavelengths although multi-wavelength samples over several square degrees e.g. in well-studied fields like COSMOS, are now enabling selection of luminous, dusty quasars at X-ray and infrared wavelengths (Brusa et al. 2010). In ULASJ1234+0907, the $A_V = 6$ mag at $z = 2.5$ corresponds to 17.5 mag of extinction in the observed-frame optical *i* band. In other words, the quasar flux is suppressed by a factor of $\sim 10^7$ at optical wavelengths due to absorption by dust, making it invisible in even the deepest optical surveys coming up within the next decade.

Highly reddened type 1 quasars like ULASJ1234+0907 that are accreting at close to the Eddington limit are distinct from the well-studied obscured type II AGN population. The FeK emission at rest frame 6.4 keV (observed frame 1.8 keV) in the quasar spectrum in Fig. 3 is only marginally detected. The X-ray spectrum of ULASJ1234+0907 is therefore markedly different from typical Compton thick sources like NGC1068, where the FeKα line is much more prominent in the reflection-dominated spectrum, and the photon index is considerably less steep (Iwasawa, Fabian & Matt 1997).

3.3 Evidence against lensing

We have demonstrated that ULASJ1234+0907 is among the brightest and reddest broad-line quasars currently known with extremely high luminosities measured at both FIR and X-ray wavelengths. Given these extreme luminosities, we should consider the possibility of the quasar being lensed. The strongest evidence against lensing is provided by our deep *i*- and *K*-band observations (Section 2). The optical image goes down to a magnitude limit of $i_{AB} < 25.15$. Even a high-redshift galaxy lens at $z > 1$ should have been easily visible at these depths. The quasar is undetected in the *i* band and there are no other galaxies present within a 7 arcsec radius of the quasar position in this *i*-band image so there is no evidence to support the presence of a galaxy lens.

The *K*-band data from ISAAC were taken in ∼0.5 arcsec seeing which would allow us to easily resolve multiple emission sources associated with lensed images of the quasar, should they have been present. From Fig. 1, we see that there is no evidence for multiple images in these subarcsecond seeing *K*-band data. The *K*-band emission from the quasar is unresolved and consistent with the size of the PSF. The lensing cross-section is therefore extremely small and the probability of lensing very low.

4 DISCUSSION AND CONCLUSIONS

The above suite of multiwavelength observations has allowed us to build up a comprehensive picture of the properties of ULASJ1234+0907, the reddest broad-line quasar currently known. With an X-ray luminosity of $L_{(2-10)\,\mathrm{keV}} = 1.3 \times 10^{45}\,\mathrm{erg\,s^{-1}}$ and a total infrared luminosity of $L_{\mathrm{TIR}} = 3.1 \times 10^{47}\,\mathrm{erg\,s^{-1}}$, ULASJ1234+0907 is among the most luminous quasars known at both these wavelengths. Through subarcsecond, deep imaging of the quasar in the *i* and *K* bands, we demonstrate that no galaxy lens is apparent in the optical and that the quasar emission is unresolved in the *K* band. Lensing is therefore unlikely to be responsible for the extreme luminosities of this source. Even accounting for a large (62 per cent) contribution of the AGN to the total infrared luminosity or assuming that only the FIR luminosity between 40 and 300 μm is powered by a starburst, the estimated SFR in the host galaxy of this quasar is $>2000\,\mathrm{M_\odot\,yr^{-1}}$. Measuring the AGN bolometric luminosity directly from the hard X-ray luminosity (assuming a bolometric correction of 100) and therefore requiring the rest of the total infrared emission to be powered by a starburst gives an even more extreme SFR of $\sim 6800\,\mathrm{M_\odot\,yr^{-1}}$. The column density inferred from the X-ray spectrum is $N_{\mathrm{H}} = 9.0 \times 10^{21}\,\mathrm{cm^{-2}}$ corresponding to $A_{\mathrm{V}} = 6$.

Cosmological simulations predict the existence of a high Eddington ratio, luminous, reddened quasar phase which marks the transition of massive starburst galaxies to UV-luminous quasars. This phase is distinct from the well-known type II obscured AGN (Hopkins et al. 2008). During this phase, the bolometric output of both the starburst and AGN are expected to be at their peak. ULASJ1234+0907 has all the observed properties expected, were it to be detected during this transition phase – high luminosity and Eddington ratio, significant dust reddening, broad emission lines and reprocessed dust emission at FIR wavelengths. This quasar is an order of magnitude more luminous than the well-studied submillimeter galaxies (SMGs) and dust-obscured galaxies which have typically been selected over much smaller areas with *Spitzer* and/or SCUBA imaging. The black hole mass is also considerably larger than measured in SMGs (B12). In terms of luminosity and space density, ULASJ1234+0907 is better matched to the new population of HyLIRGs discovered using the *WISE* All Sky Survey (Eisenhardt et al. 2012), although drawing evolutionary links between the *WISE* HyLIRGs and dust-reddened type 1 quasars would require detailed consideration of the relative lifetimes of these two phases, which is beyond the scope of this work. We emphasize that reddened type 1 quasars like ULASJ1234+0907 are distinct from the more highly obscured and less luminous type II AGN where the dust extinction can often be explained by orientation effects. We have provided some evidence that the dust extinction in ULASJ1234+0907 arises on larger scales in the quasar host galaxy thus allowing the broad-line region to be viewed in the NIR. This dust is likely heated by both the AGN and a powerful starburst as would be expected during blowout. Although our observations do not directly detect AGN-driven outflows, the combination of an SMBH accreting at close to the Eddington limit coupled with the high column density is expected to drive strong outflows due to the effects of radiation pressure on dust.

The reddened quasar phase is unique in allowing us to study both the central accreting power source (through X-ray and NIR spectroscopy) and the starburst host galaxy (through FIR photometry) in massive galaxies observed at the peak epoch of galaxy and black hole formation. We are assembling multiwavelength observations of much larger samples of these highly reddened type 1 quasars which will inform theories of massive galaxy formation and be ideal testbeds for studying AGN feedback.

ACKNOWLEDGEMENTS

MB would like to thank Paul Hewett for many useful discussions. We thank Matt Auger for discussions on lensed quasars, Eduardo Gonzalez-Solares for help with the INT data reduction and Maud Galametz for tips on *Herschel* data reduction. This work is based on observations made with *XMM–Newton*, an ESA science mission with instruments and contributions directly funded by ESA Member States and NASA and the ESO telescopes at the La Silla Paranal Observatory under programme ID: 290.A-5062.

REFERENCES

Banerji M., McMahon R. G., Hewett P. C., Alaghband-Zadeh S., Gonzalez-Solares E., Venemans B. P., Hawthorn M. J., 2012, MNRAS, 427, 2275 (B12)
Banerji M., McMahon R. G., Hewett P. C., Gonzalez-Solares E., Koposov S. E., 2013, MNRAS, 429, L55 (B13)
Bendo G. J. et al., 2013, MNRAS, 433, 3062
Brusa M. et al., 2010, ApJ, 716, 348
Casey C. M., 2012, MNRAS, 425, 3094
Coppin K. E. K. et al., 2008, MNRAS, 389, 45
Croton D. J. et al., 2006, MNRAS, 365, 11
Cutri R. M. et al., 2012, VizieR On-line Data Catalog: II/311. Originally published in: 2012yCat, Technical report, Explanatory Supplement to the WISE All-Sky Data Release Products
Dale D. A., Helou G., 2002, ApJ, 576, 159
Davies J. I. et al., 2010, A&A, 518, L48
Di Matteo T., Springel V., Hernquist L., 2005, Nature, 433, 604
Eisenhardt P. R. M. et al., 2012, ApJ, 755, 173
Elvis M. et al., 1994, ApJS, 95, 1
Fabian A. C., 2012, ARA&A, 50, 455
Fritz J., Franceschini A., Hatziminaoglou E., 2006, MNRAS, 366, 767
González-Solares E. A. et al., 2011, MNRAS, 416, 927
Gregg M. D., Lacy M., White R. L., Glikman E., Helfand D., Becker R. H., Brotherton M. S., 2002, ApJ, 564, 133
Hewett P. C., Warren S. J., Leggett S. K., Hodgkin S. T., 2006, MNRAS, 367, 454
Hickox R. C. et al., 2012, MNRAS, 421, 284
Hopkins P. F., Hernquist L., Cox T. J., Kereš D., 2008, ApJS, 175, 356
Iwasawa K., Fabian A. C., Matt G., 1997, MNRAS, 289, 443
Jansen F. et al., 2001, A&A, 365, L1
Kennicutt R. C., Evans N. J., 2012, ARA&A, 50, 531
Magorrian J. et al., 1998, AJ, 115, 2285
Mullaney J. R., Alexander D. M., Goulding A. D., Hickox R. C., 2011, MNRAS, 414, 1082
Noll S., Burgarella D., Giovannoli E., Buat V., Marcillac D., Muñoz-Mateos J. C., 2009, A&A, 507, 1793
Pilbratt G. L. et al., 2010, A&A, 518, L1
Poglitsch A. et al., 2010, A&A, 518, L2
Polletta M. et al., 2007, ApJ, 663, 81
Priddey R. S., Isaak K. G., McMahon R. G., Omont A., 2003, MNRAS, 339, 1183
Raimundo S. I., Fabian A. C., Bauer F. E., Alexander D. M., Brandt W. N., Luo B., Vasudevan R. V., Xue Y. Q., 2010, MNRAS, 408, 1714
Roussel H., 2012, PASP, 125, 1126
Rowan-Robinson M., 2000, MNRAS, 316, 885
Smail I., Swinbank A. M., Ivison R. J., Ibar E., 2011, MNRAS, 414, L95
Urrutia T., Lacy M., Becker R. H., 2008, ApJ, 674, 80
Wang R. et al., 2010, ApJ, 714, 699

This paper has been typeset from a TEX/LATEX file prepared by the author.